Int. J. Electrochem. Sci., 17 **(2022)** Article Number: 220711, doi: 10.20964/2022.07.18

International Journal of
ELECTROCHEMICAL
SCIENCE
www.electrochemsci.org

Corrosion Behavior of A413/SiC Composites Produced by Mechanical Alloying

Ociel Rodríguez Pérez[1], *J. A. García-Hinojosa*[1], *F. J. Rodríguez-Gómez*[1], *Roy Lopez-Sesenes*[3], *Cesar A. Garcia-Pérez*[2], *R. Guardián Tapia*[2], *J.G. Gonzalez-Rodriguez*[2,*]

[1] Departamento de Ingeniería Metalúrgica, Facultad de Química, Universidad Nacional Autónoma de México, Circuito Exterior, Ciudad Universitaria, 04510, México
[2] Centro de Investigación en Ingeniería y Ciencias Aplicadas-IICBA, UAEM, Avenida Universidad 1001, 62209, Cuernavaca, Morelos, México
[3] Facultad de Ciencias Quimicas e Ingeniería, UAEM, Avenida Universidad 1001, 62209, Cuernavaca, Morelos, México
[*]E-mail: ggonzalez@uaem.mx

Received: 23 February 2022 / *Accepted:* 28 April 2022 / *Published:* 6 June 2022

The corrosion behaviour of A413/SiC composites with different SiC contents (5, 10, and 15 wt.%) was evaluated through electrochemical techniques in 3.5 wt.% NaCl solution. For this purpose, composites were produced by the mechanical alloying technique. In addition to this, X-ray diffraction and by Scanning electronic microscope studies were performed. It was found that the addition of SiC increased both density and porosity. Electrochemical tests showed that the corrosion resistance of unreinforced A413 alloy was improved with the addition of 5% SiC but the addition of either 10 or 15 % SiC was detrimental. The corrosion products film developed on top of unreinforced A413 alloy and composite containing 5 % SiC consisted basically of protective Al_2O_3, alumina layer, whereas that formed on top of composites containing either 10 or 15 % SiC contained less Al as well as Fe and Cr making them less protective.

Keywords: A413/SiC composites, electrochemical techniques, corrosion, mechanical alloying.

1. INTRODUCTION

A413 aluminum alloy is well known for its excellent castability, good dimensional stability, high corrosion resistance, good weldability, pressure tightness, and specific strength [1, 2]. Due to these properties, this alloy is widely used in order to replace steel components in automotive, aircraft, and military industries. Main applications of A413 aluminum alloy include the manufacture of components such as pistons, connecting rods, housings, cylinders, blocks, compressors, switch boxes, road transport fittings, and marine fittings [3, 4]. A413 aluminium alloy is also used as the matrix for obtaining

composites with oxides, carbides, and some intermetallic compounds. Reinforcements such as TiC, Al_2O_3, SiC, B_4C, Ashes, Al-Al_3Ti, Al-TiB_2, etc. have been used by different researchers [5-9] to synthesize aluminum matrix composites (AMCs). Among the different reinforcements, silicon carbide (SiC) has been chosen for this study due to its low density, high melting point, oxidation resistance, low cost, good thermal stability, high hardness, and wear resistance. The physical, chemical and mechanical properties of AMCs can be affected by the type of fabrication technique, process parameters and characteristics of the reinforcement phase used. Nowadays, there are different methods to produce the AMCs such as squeeze [10] and stir casting [11], liquid metal infiltration [12], mechanical alloying [13], and powder metallurgy [14]. Mechanical alloying (MA) is a powder processing technique in a high energy ball mill that leads to repeated plastic deformation, cold welding, fracturing, and re-welding of the alloying elements with reinforcement particles forming the alloyed powder.

Mechanical alloying technique with the appropriate processing parameters favours a homogeneous distribution of the alloying elements with the reinforcing materials [15, 16]. The surface of the aluminium alloy has a natural thin oxide film (Al_2O_3) which stops the oxidation process, giving it resistance to corrosion and durability. However, when there are Cl^- ions, their passivation disappears and it is very reactive.

However, one of the main disadvantages of the addition of reinforcement particles in AMCs is their influence on corrosion behaviour. The reinforcement phase makes it difficult to protect the passive film due that reinforcement introduces inhomogeneities on the surfaces exposed to aggressive environments. The corrosion resistance of the composites also depends upon the type, size, and amount of reinforcement added.

Corrosion resistance is an important property that should be taken into account during the materials selection for industrial applications and avoid damage such as operation failure. Previous studies about corrosion behaviour on AMCs have been focused on the effect of SiC content. Wang et al. [17], for instance, studied the corrosion behaviour of mechanically alloyed SiC/2014Al composites in a 3.5% NaCl solution. Results showed that the corrosion current density value of composite layer with 3 vol.% n-SiCp was much lower than that of 2014Al matrix, however, the corrosion current density value for composite layer with 7 vol.% was higher than the 2014Al matrix. Niveen et al. [18] evaluated the electrochemical corrosion behaviour of SiC nanoparticles based AA6061 aluminium alloy in 3.5% NaCl solution. The results showed that the corrosion rate decreased with an increase of the percentage of the SiC particles. Sahib et al. [19] studied the corrosion behaviour of Al/SiC composite prepared by powder metallurgy varying proportions 10 and 20% wt. SiC. Composites rate of corrosion was measured using the potentiodynamic polarization technique in chloride environments of 0.5 M hydrochloric acid and 0.5 M sodium chloride solutions. It was found that by increasing the wt.% SiC of the Al/SiC composite contributed a higher corrosion rate in both solutions. Aruna et al. [20] evaluated the corrosion behaviour of SiC-Al_20_3 composites in 3.5 % NaCl solution, finding that the corrosion products protective film can be disrupted by heterogeneities due to the existence of reinforcing phase in the composite material and, thus, with an increase in the corrosion rate due to an increase in the number of active of active sites. Another research works have reported similar results [21-26] due to the formation of discontinuities between the matrix and the reinforced particulates as well as the formation of micro galvanic cells which leads to a higher susceptibility to localised type of corrosion such as pitting and crevice corrosion.

The fact is that from the literature review there are many aluminium alloys with reinforcements combinations which might present a completely different corrosion behaviour. This study is an effort to understand the corrosion behavior of unreinforced and reinforced A413 (5, 10, and 15 wt.%) SiC composites produced by mechanical alloying (MA) technique and uniaxially pressing/sintering route. For this purpose, prepared samples were evaluated by using electrochemical and surface analysis techniques in 3.5 wt.% NaCl solution.

2. EXPERIMENTAL PROCEDURE

2.1. Materials

In the current study, A413aluminium alloy powder (density of 2.66 g/cm^3, <60 Mesh) was used as matrix material. The chemical composition of aluminium A413 alloy powder is shown in table 1.

Table 1. Chemical composition of aluminum A413 alloy (wt.%).

Al	Si	Fe	Cu	Mn	Mg	Cr	Ni	Zn	Ti	Pb	Sn
Bal.	11.69	0.75	0.28	0.23	0.06	0.021	0.015	0.280	0.027	0.005	0.002

Silicon carbide particles (density of 3.21 g/cm^3, an average particle size of 38 μm, Aldrich, 97.5 %) were used to reinforce the A413 alloy matrix.

2.2. Composites preparation

The A413/SiC composites were produced by mechanical alloying technique as follows: the proper proportions of both A413 alloy powders and silicon carbide particles (5, 10, and 15 wt.% SiC) were milled in a Fritsch–P7 ball mill during 10 h at a speed of 300 rpm under a no-oxidant atmosphere. Stearic acid was used as a process control agent (PCA). The ratio between the milling ball and the powder weight ratio (BPR) was 5:1. The obtained powders were uniaxially cold compacted at 600 MPa in tool steel die, obtaining specimens 10 mm in diameter, and 5 mm in height. Finally, specimens were sintered at 500 ˚C during 4 h under an argon atmosphere. Also, an unreinforced A413 aluminum alloy was produced by the same route for comparative purposes. Specimens were characterized by a low vacuum LEO Scanning electronic microscope (SEM) whereas X-ray diffraction of the consolidated samples was carried out by D2 PHASER a mobile bench top X-ray diffractometer (XRD). Archimedes method was used in order to obtain experimental density (ρEX), while the theoretical density (ρT) was calculated according to Eq. 1.

$$\rho T = (wt._{matrix} * \rho_{matrix}) + (wt._{SiC} * \rho_{SiC}) \qquad (1)$$

where, ρT = Theoretical density, $wt._{matrix}$ = weight fraction of A413, ρ_{matrix} = density of A413, $wt._{SiC}$ = weight fraction of SiC, and ρ_{SiC}= density of SiC. The percent porosity of the samples was determined in accordance with [25] using the Eq. 2.

$$\% \, Porosity = \{(\rho T - \rho EX)/\rho T\} \times 100\% \quad (2)$$

where, ρT = Theoretical density (g/cm^3), and ρEx = Experimental density (g/cm^3).

2.3. Electrochemical tests

Electrochemical techniques including potentiodynamic polarization curves, electrochemical impedance spectroscopy (EIS), and linear polarization resistance (LPR) measurements were used in a 3.5 % NaCl solution at room temperature (25 ºC) by using an ACM Instruments potentiostat. A normally aerated glass cell electrochemical cell was used for this with a saturated calomel electrode (SCE) as a reference and a 6 mm diameter graphite rode as a counter electrode. Composite samples were used as a working electrode using an alligator clip with wire and encapsulated one face of the sample with commercial epoxy resin. Before each testing, samples surfaces were ground by using 600 silicon carbide emery paper in accordance with ASTM standard [26] and then cleaned with deionized water followed, rinsing with ethanol and dried in air. Specimens were allowed to stabilize at open circuit potential (OCP) during a period of 30 min before starting the electrochemical tests. Before starting the polarization curves, specimens were polarized at a potential value of 500 mV more cathodic than the free corrosion potential value, E_{corr}, scanned towards the anodic direction ata scan rate of 1 mV/s ending at a potential value 1000 mV more anodic than E_{corr}. Tafel extrapolation method was used in order to calculate corrosion current density values, I_{corr}. LPR experiments were carried out at the Ecorr value and polarizing the specimen ±10 mV every 60 min during 24 hours at a scan rate of 1 mV/s. Finally, EIS experiments were performed at the E_{corr} value by polarizing the specimen ±15 mV at the frequency interval from 0.01 Hz to 100 kHz. All tests were repeated three times under the same conditions to guarantee the reproducibility of the data. EIS technique were performed using a Gamry PC4 300 potentiostat. Microstructural characterization of the composites samples, before and after the corrosion tests were performed by LEO SEM whereas micro chemical analysis was carried out by using an Energy dispersive x-ray analyser (EDX) attached to it.

3. RESULTS AND DISCUSSION

3.1 Microstructural characterization

Fig. 1 shows the SEM micrographs of the as-received unreinforced A413 alloy and A413/SiC composites containing 5, 10, and 15 wt.% of SiC. The microstructure of consolidated samples shows the existence of porosity which increases with an increase in the SiC particles content into the A413 alloy matrix.

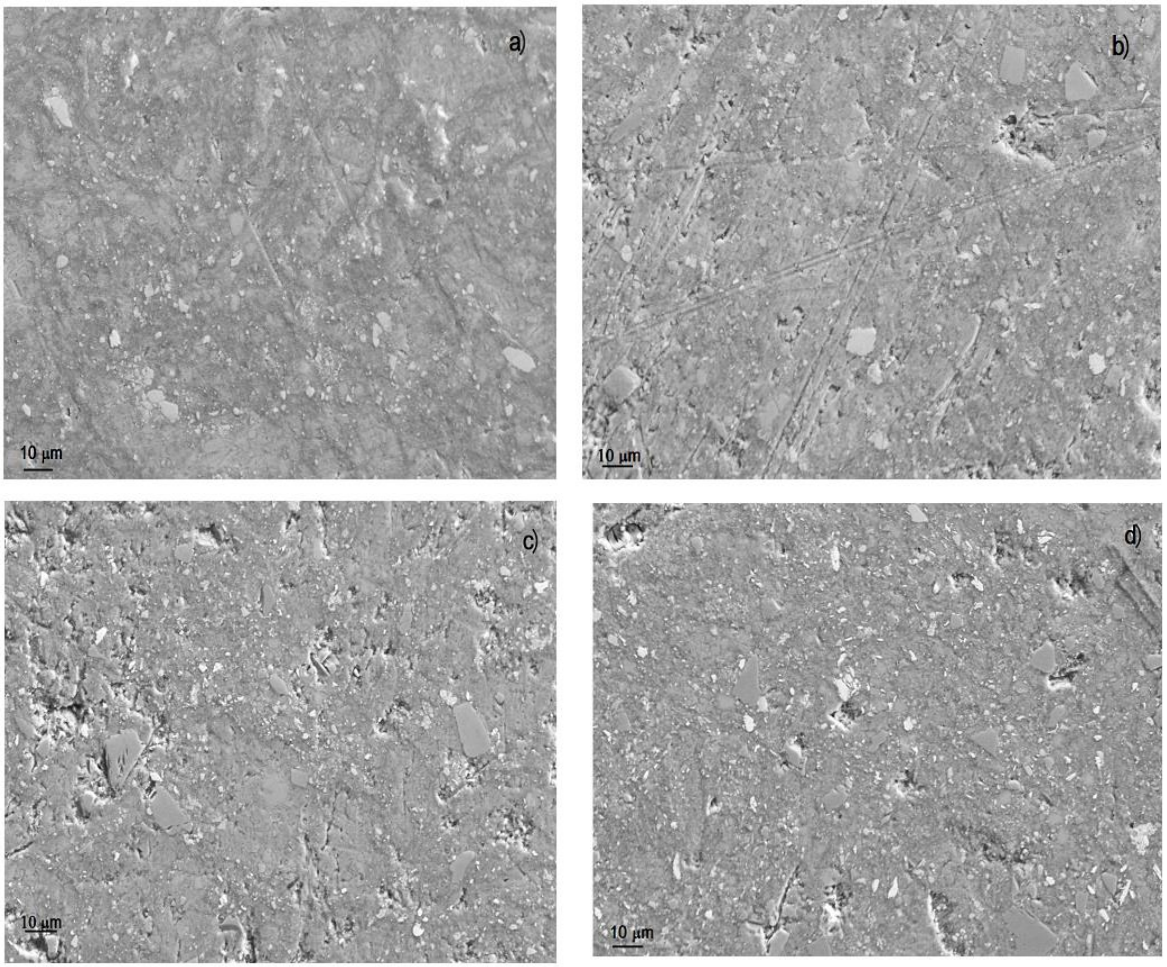

Figure 1. SEM images of as-received a) unreinforced A413 alloy, b) A413-5 wt.% SiC, c) A413-10 wt.% SiC, and d) A413-15 wt.% SiC composites.

Table 2. Density and percent porosity of the consolidated samples

Sample	Theoretical density (g/cm^3)	Experimental density (g/cm^3)	Porosity (%)
Unreinforced A413 alloy	2.686	2.62 ± 0.01	2.45
A413-5 wt.% SiC	2.7127	2.63 ± 0.02	2.93
A413-10 wt.% SiC	2.7394	2.64 ± 0.02	3.62
A413-15 wt.% SiC	2.7661	2.65 ± 0.01	3.98

It can be seen that the surface of the unreinforced A413 alloy, Fig. 1 a, exhibited the lowest porosity content among all the samples. The surface composite with 15 wt.% SiC shows the highest porosity content with visible evidence of SiC reinforcement particles angular in shape and sharp edges Fig. 1 d. SEM images show that the porous have irregular shapes and different sizes. Also, SEM micrographs show that the SiC particles have a good bonding with the A413 alloy matrix by the mechanical alloying technique.

The density and porosity of the consolidated samples for different SiC concentrations are given in table 2. It is observed that the density and porosity of composites are generally higher as compared to those for unreinforced A413 alloy. The experimental density reported shows lower values than the expected theoretical density value due to the porosity formation in the samples. Also, the theoretical density, experimental density and porosity of the samples increase as the weight percent of the SiC particles increases into the A413 alloy. A similar observation about the increased porosity of Al/SiC composite by the addition of SiC particles has been reported by other researchers [27]. Composite containing 15 wt.% SiC had the highest experimental density value of 2.656 g/cm^3 and the maximum porosity measure of 3.98 %. The fact that the porosity increases in the composite samples is due in part to the manufacturing process parameters such as the pressure of compaction, time and temperature of sintering, both shape and size of particle, and weight fraction of particle. The composite systems that contains a higher number of silicon carbide particles will be affected due to the fact that hard silicon carbide particles reduce the compressibility of the powders, creating more porosity with irregular shapes.

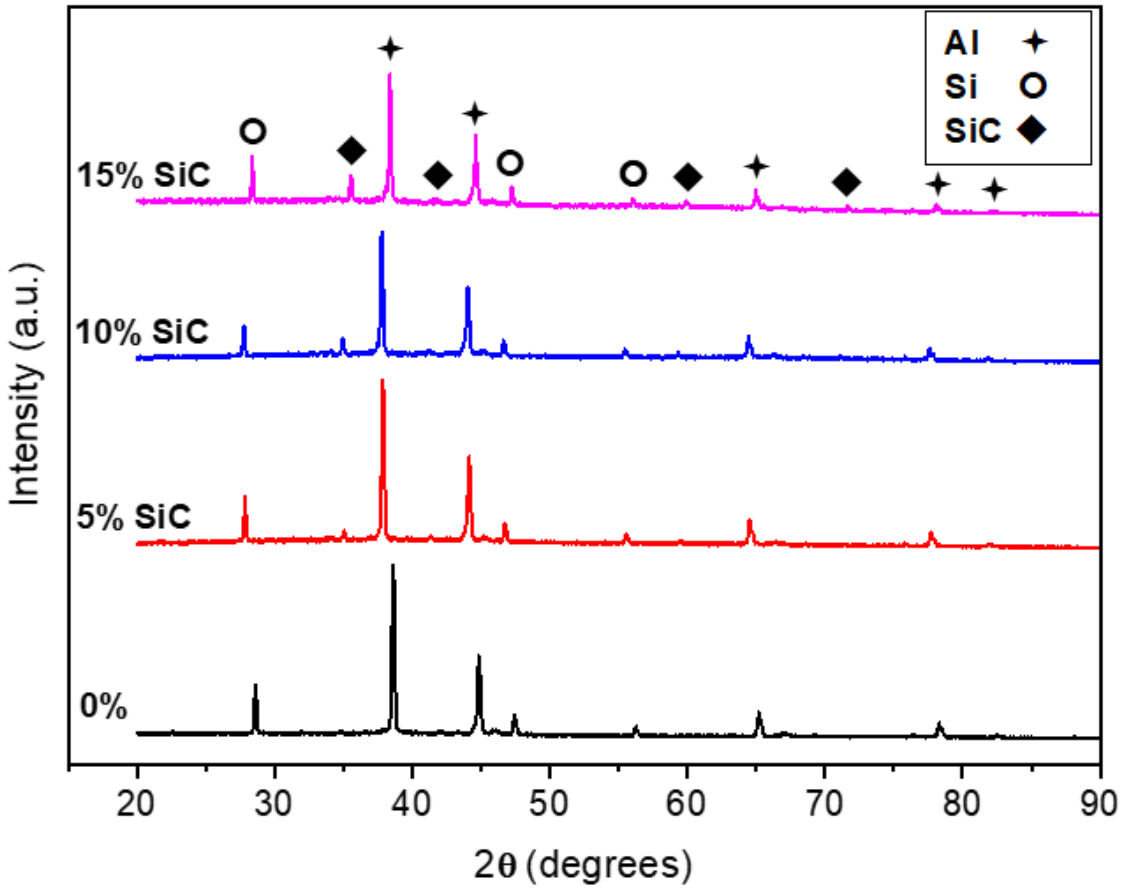

Figure 2. XRD patterns of A413/SiC composites samples as a function of the SiC content.

XRD patterns of unreinforced A413 aluminium alloy and A413/SiC composites are shown in Fig. 2. The patterns of the reinforced composites reveal that the principal peak intensities correspond to aluminium (Al), silicon (Si), and silicon carbide (SiC) phases. The Al peaks are located approximately at 2θ= 38.60, 44.84, 65.17, 78.29, and 82.47. Si peaks are located at values for 2θ= 28.60, 47.45, and

56.28. Finally, the SiC peaks are located at values for 2θ= 35.53, 41.85, 59.91, and 71.65. The diffraction peaks of Si and SiC have lower intensity than those corresponding to Al, due to the lower weight percentages of these phases in the composites samples. As expected, the unreinforced A413 aluminium alloy that was produced as a reference sample differs from the composites by not showing the presence of SiC peaks intensity. Moreover, the peaks intensity belonging to the SiC in the composites gradually increased as the weight fraction of SiC particles increased, indicating a good distribution of the reinforcing particles in the matrix alloy. Additionally, no secondary phases were observed in the XRD patterns.

3.2 Electrochemical tests

Polarization curves for A413 aluminium alloy in 3.5 NaCl solution at different contents of SiC contents is given in Fig. 3, whereas their electrochemical parameters such as E_{corr}, I_{corr}, pitting potential value, E_{pit}, and passivation current density value, I_{pas}, are summarized in table 3.

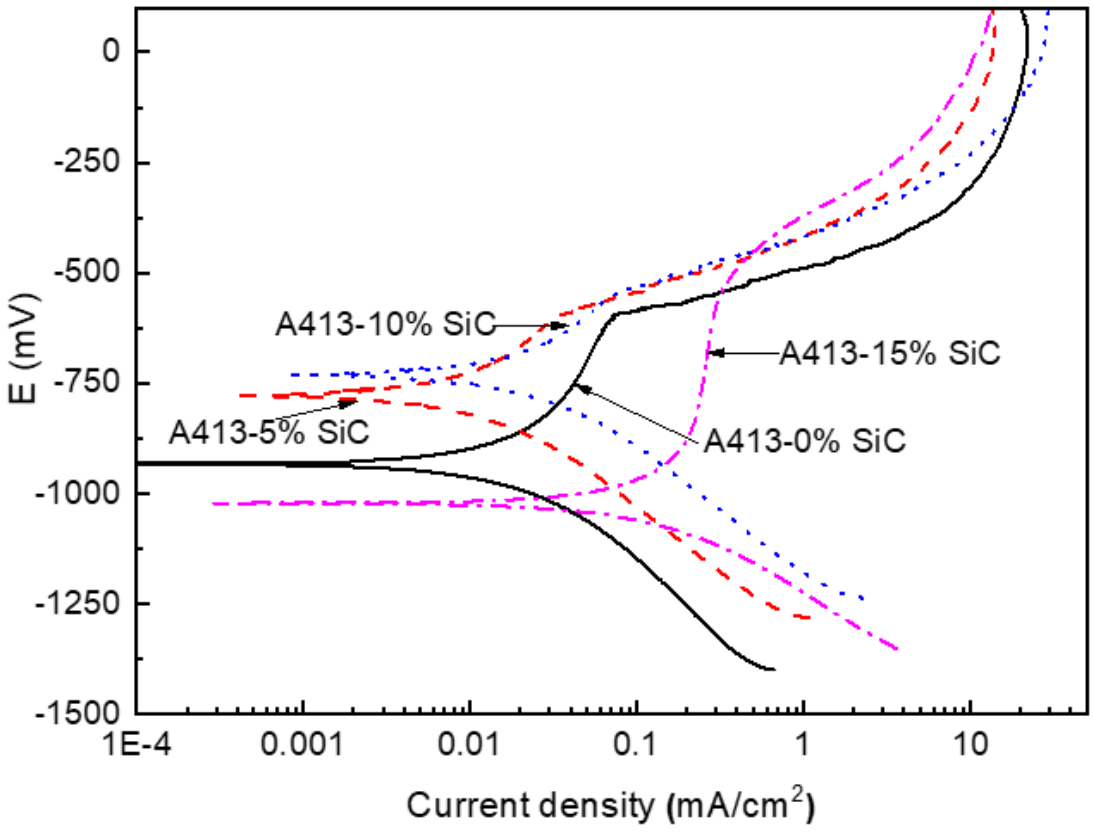

Figure 3. Polarization curves for the A413/SiC composites at different SiC contents and corroded in 3.5 NaCl solution.

Table 3. Electrochemical parameters extracted from polarization curves.

Sample designation	E_{corr} (mV)	I_{corr} (mA/cm^2)	E_{pit} (mV)	I_{pas} (mA/cm^2)
Unreinforced A413 alloy	-930	0.025	-590	0.044
A413-5% SiC	-775	0.009	-620	0.023
A413-10% SiC	-725	0.023	-560	0.037
A413-15% SiC	-1015	0.148	-515	0.257

Data for unreinforced A413 aluminium alloy depicts an active-passive behaviour. When the polarization starts on the cathodic branch of the curve, cathodic current is due to the oxygen reduction reaction, which starts to decrease as the potential approaches the E_{corr} value. From this point and as the anodic potential increases, anodic current density value increases rapidly due to the dissolution of Al, until a passive layer is formed due to the formation of an Al_2O_3 layer, where current density value remains more or less constant, and when a breakdown or pitting potential is reached and the current shows an abrupt increase. The region where there is a rapid increase in the anodic current density, before the establishment of the passive layer, due to the rapid dissolution of Al occurs according to following reaction [28-29]:

$$Al \rightarrow Al^{3+} + 3e^- \quad (3)$$

whereas cathodic oxygen reduction reaction occurs according to [30]:

$$O_2 + 2H_2O + 4e^- \rightarrow 4OH^- \quad (4)$$

Reaction of OH^- ions and its adsorption on to the metallic surface of Al-SiC composite forms an hydroxide film, with the formation of the passive layer, according to:

$$Al^{3+} + 3OH^- \rightarrow Al(OH)_3 \quad (5)$$

but, since $Al(OH)_3$ is very unstable, it transforms in to hydrated Al_2O_3 as follows:

$$Al(OH)_3 \rightarrow Al_2O_3 \bullet 3H_2O \quad (6)$$

The presence of presence of SiC as reinforcement did not affect the passive behavior of the alloy, however, as shown in table 3, the E_{corr} value became nobler with the addition of 5 and 10 % SiC, but it became more active with the addition of 15 % SiC. The presence of SiC particulates are sites for the disruption of the passive layer, and that they act as cathodic zones as compared with the matrix, which acts as anodes and, thus, leading to a galvanic attack. Although the passive layer can be disrupted by these particles, once they are exposed to the electrolyte, they are detached from the surface and washed away, the accumulation of corrosion products leads to the formation of the passive layer once again [30-33]. However, on the sites where the SiC particles were detached, localized type of corrosion such as

pits can occur which is caused by the presence of heterogeneities such as grain boundary, intermetallic, reinforcement/matrix interface, inclusion, defect, etc.

Table 4. Parameters obtained from the fitting of EIS data.

Sample designation	R_s (ohm cm^2)	C_f (F cm^2)	R_f (ohm cm^2)	C_{dl} (Fcm^2)	R_{ct} (ohm cm^2)
Unreinforced A413 alloy	9	3.80×10^{-4}	222	6.50×10^{-4}	988
A413-5% SiC	6	1.49×10^{-4}	504	9.65×10^{-5}	1180
A413-10% SiC	7	5.69×10^{-4}	233	2.52×10^{-4}	672
A413-15% SiC	4	8.45×10^{-4}	179	3.62×10^{-3}	243

Similarly, the I_{corr} value decreased when 5 % SiC was added as reinforcement, remained virtually unaltered with the addition of 10 % SiC and it increased with the addition of 15 % SiC.

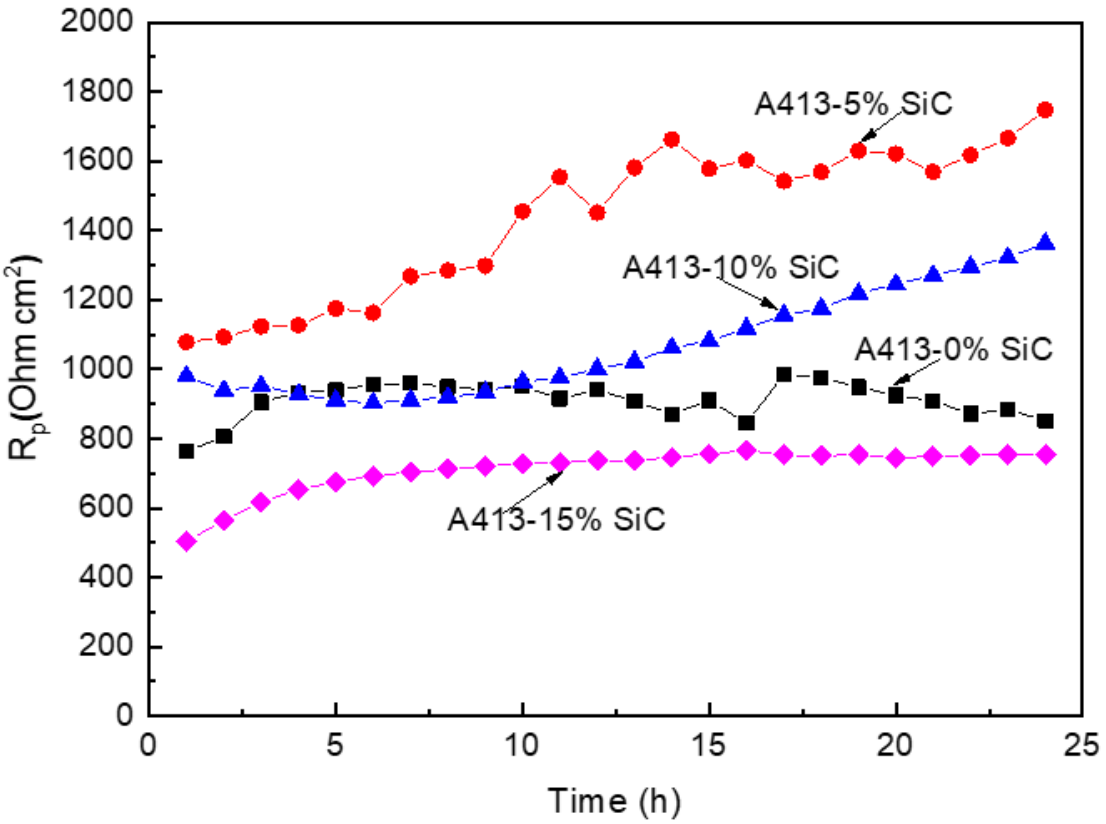

Figure 4. Variation on the R_p value with time for the A413/SiC composites samples as a function of SiC content and corroded in 3.5 NaCl solution.

The pitting potential value, E_{pit}, increased towards nobler values when 5 % SiC was added, but it went towards more negative with the addition of either 10 or 15% SiC. Passive current density value, I_{pas}, it decreased with the addition of either 5 or 10 % SiC, but it increased with the addition of 15 %

SiC. Thus, all the evidence shows that the best corrosion performance is obtained with the addition of 5% SiC, but it is deteriorated with an increase in the SiC contents. A similar behavior was obtained by Wang et al. [17] when evaluating 2014Al/SiC composites containing 1, 3, 5 and 7 wt. % SiC nano particulates in 3.5 % NaCl solution. The I_{corr} value of unreinforced Al 2014 alloy was decreased with the addition of either 1, 3 or 5 % SiC, but it was increased with a further increase in the SiC nano particulates contents. They explained this behaviour due to the precipitation of electrically conductive Al_2Cu particulates, especially in the composites containing either 1 or 3% SiC, but almost disappeared as the SiC contents increased further. These particulates acted as cathodes to the aluminium matrix.

In order to know the evolution with time of the composites corrosion behaviour, LPR experiments were carried out during 24 hours of testing, taking the linear polarization resistance value, R_p, as main parameter, since according to the Stern-Geary equation, corrosion current density and the R_p values are inversely proportional:

$$I_{corr} = (\beta a.\beta c/ (2.3 (\beta a + \beta c))/R_p \quad (7)$$

where βa and βc are the anodic and cathodic Tafel slopes respectively. The higher the R_p value is, the lower is the I_{corr} value. The effect of the SiC contents on the change in the R_p value with time for the A413/SiC composites is given in Fig. 4.

This figure shows that the R_p value for unreinforced A413 alloy decreases slightly during the first 5-8 hours of testing due to the alloy dissolution, but after this time, the R_p value increases as time elapsed due to the formation of a protective $Al_2O_3 \bullet 3H_2O$ passive layer as explained above [15, 16]. For composite containing 5 % SiC, an increase in the R_p value could be observed as compared with the value observed for unreinforced A413 and it kept increasing as time elapsed. However, with an increase in the SiC up to 10 %, the R_p value was slightly higher than that obtained for unreinforced A413 alloy, showing a still higher corrosion resistance than the later. Finally, for composite containing 15 % SiC, the R_p value obtained was lower than that observed for unreinforced A413 alloy, indicating a deterioration on the corrosion resistance of metallic matrix.

EIS data, in both Nyquist and Bode formats, for unreinforced A413 alloy and A413/SiC composites are given in Fig. 5. Nyquist diagrams depict the presence of two depressed semicircles: the first one, a capacitive one, exhibited at the highest and medium frequency values, whereas a second one is visualized at the lowest frequency values, Fig. 5 a. Electron charge transfer from the metal to the electrolyte through the double electrochemical layer give rise to the high and intermediate frequency values semicircle; on the other hand, electrochemical reactions taking place at the metal/corrosion products film makes the low frequency loop to appear [34-37]. The high frequency loop diameter of the unreinforced A413 alloy increased with the addition of 5 % SiC but it decreases with a further increase in the SiC contents. On the other side, Bode plots in the modulus format shows that the total impedance or modulus increases when 5 % SiC was added to the unreinforced A413 alloy and it decreases with the addition of either 10 or 15 % SiC. Two different slopes can be seen in these plots, indicating the presence of two different time constants. On the other side, phase angle plot for unreinforced A413 alloy shows a wide frequency interval where this parameter remains more or less constant, typical of a pasivated material, due to the presence of an Al_2O_3 layer as explained above. The phase angle obtained its

maximum value, close to 50 degrees, for composite containing 5 % SiC, and it decreased with a further increase in the SiC contents.

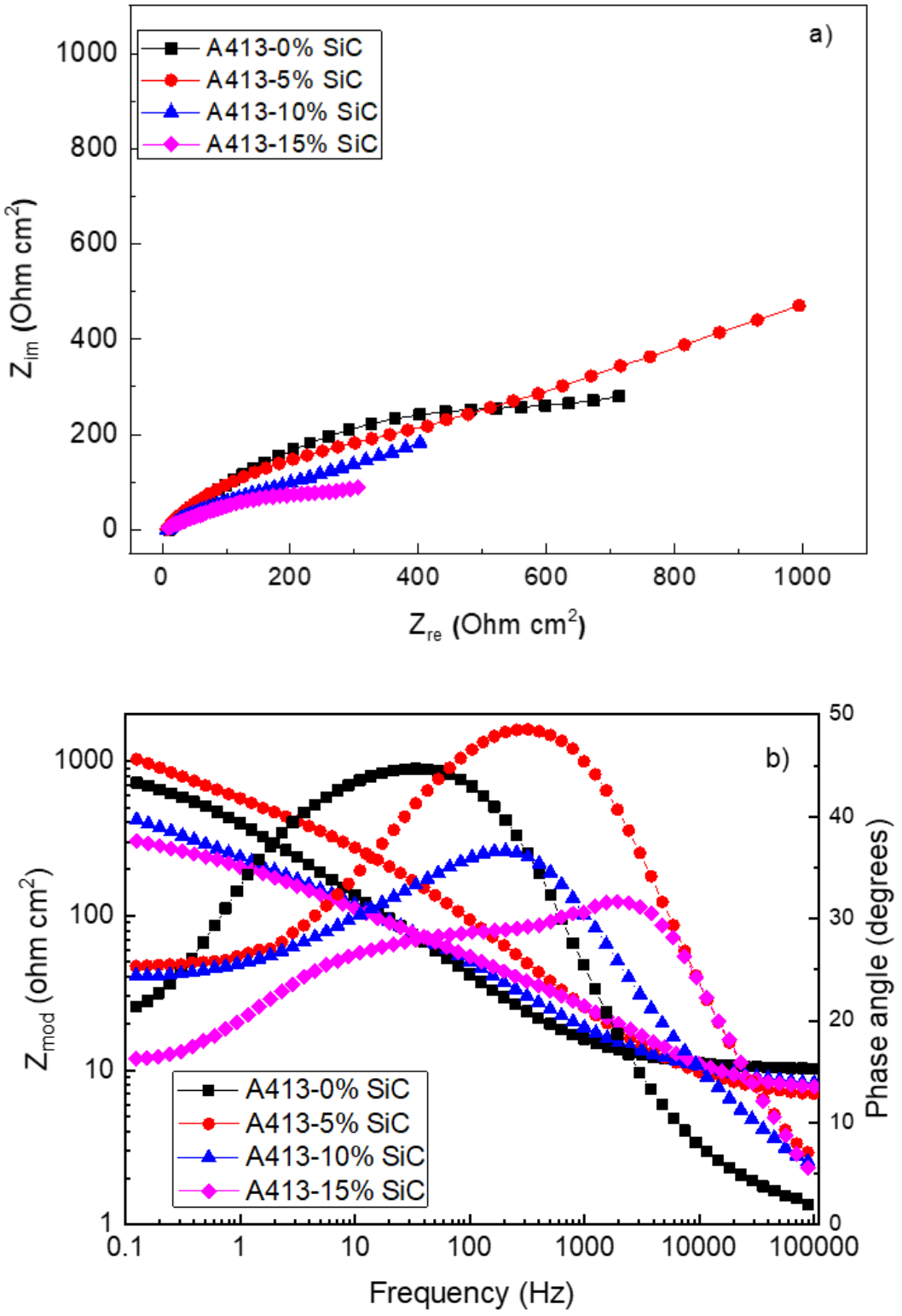

Figure 5. Effect of the SiC content on the a) Nyquist and b) Bode plots for the A413/SiC composites samples and corroded in 3.5 NaCl solution.

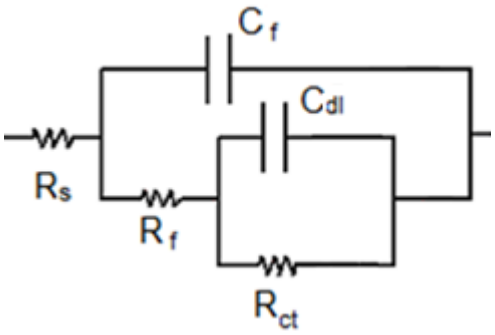

Figure 6. Electric circuit used to fit EIS data for the different A413/SiC composites.

EIS data were fitted to equivalent electric circuits as that shown in Fig. 6, where the resistance of the electrolyte or solution is represented by R_s, the corrosion products film resistance and capacitance are represented by R_f and C_f respectively; finally, the resistance and capacitance of the double electrochemical layer where the charge transfer occurs are represented by R_{ct} and C_{dl} respectively. Table 4 gives the resulting parameters obtained from fitting the experimental EIS data by using electric circuit shown in Fig.6. Table 4 shows that both, charge transfer and corrosion products film resistance values, R_{ct} anf R_f respectively, increased when 5 % SiC were added to the unreinforced A413 alloy and they decrease with the addition of either 10 or 15 % SiC. Similar results were observed for the polarization resistance values, R_p, as shown in Fig.4, indicating that highest corrosion resistance is obtained for composite containing 5 % SiC. Conversely, double layer and corrosion products film capacitance values, C_{dl} and C_f respectively, decreased when 5 % SiC were added to the unreinforced A413 alloy and their value increased with the addition of either 10 or 15 % SiC. The fact that the minimum C_{dl} value was obtained for composite containing 5 % SiC indicates that the best passive film was obtained for this composite, as it was shown in table 3 which evidenced that the highest pitting potential and lowest passive current density values were obtained for this composite.

3.3 Corroded surfaces characterization.

SEM micrographs of corroded specimens after being exposed to the 3.5 % NaCl solution after 24 hours of immersion are shown in Fig. 7.

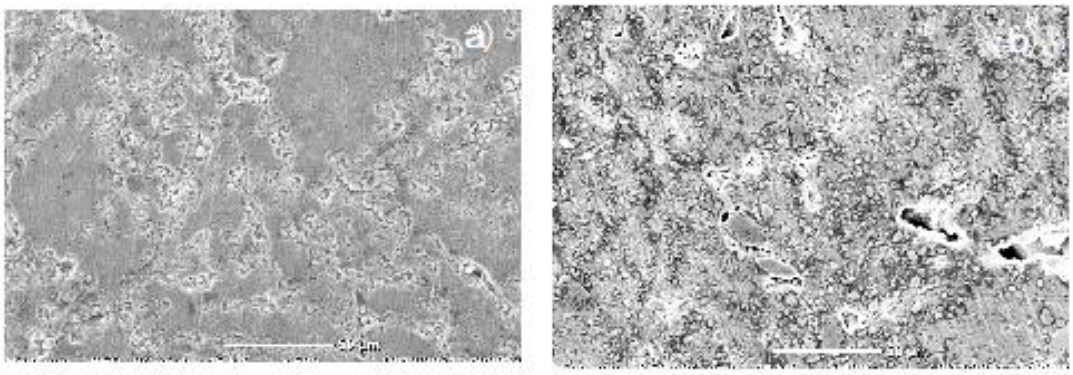

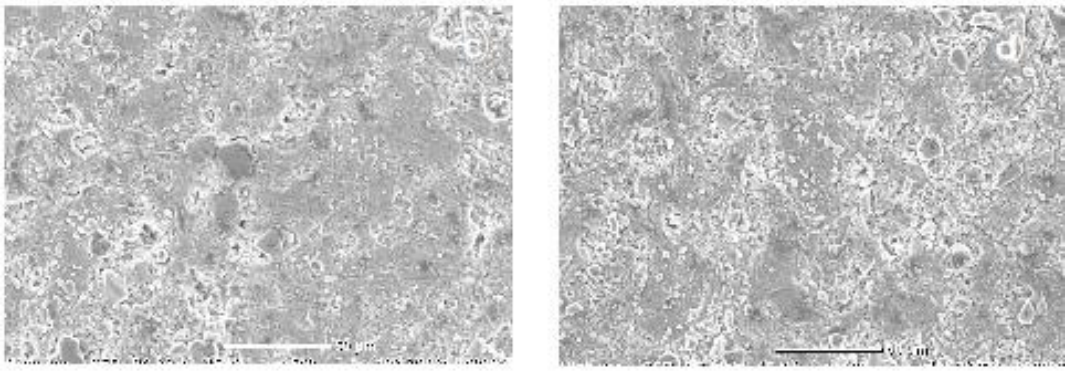

Figure 7. SEM images of a) unreinforced A413 alloy, b) A413-5 wt.% SiC, c) A413-10 wt.% SiC, and d) A413-15 wt.% SiC composites corroded in 3.5 NaCl solution.

Unreinforced A413 alloy exhibited some localised type of corrosion such as pits as well as corrosion at the interface between some particulates and matrix, Fig. 7 a. Because the metal matrix alloy form microgalvanic cells with the SiC reinforcements, composites are generally more susceptible to corrosion than corresponding matrix, causing a selective attack at the interface, where the matrix generally behaves as anode and reinforcement particulates as cathodes.

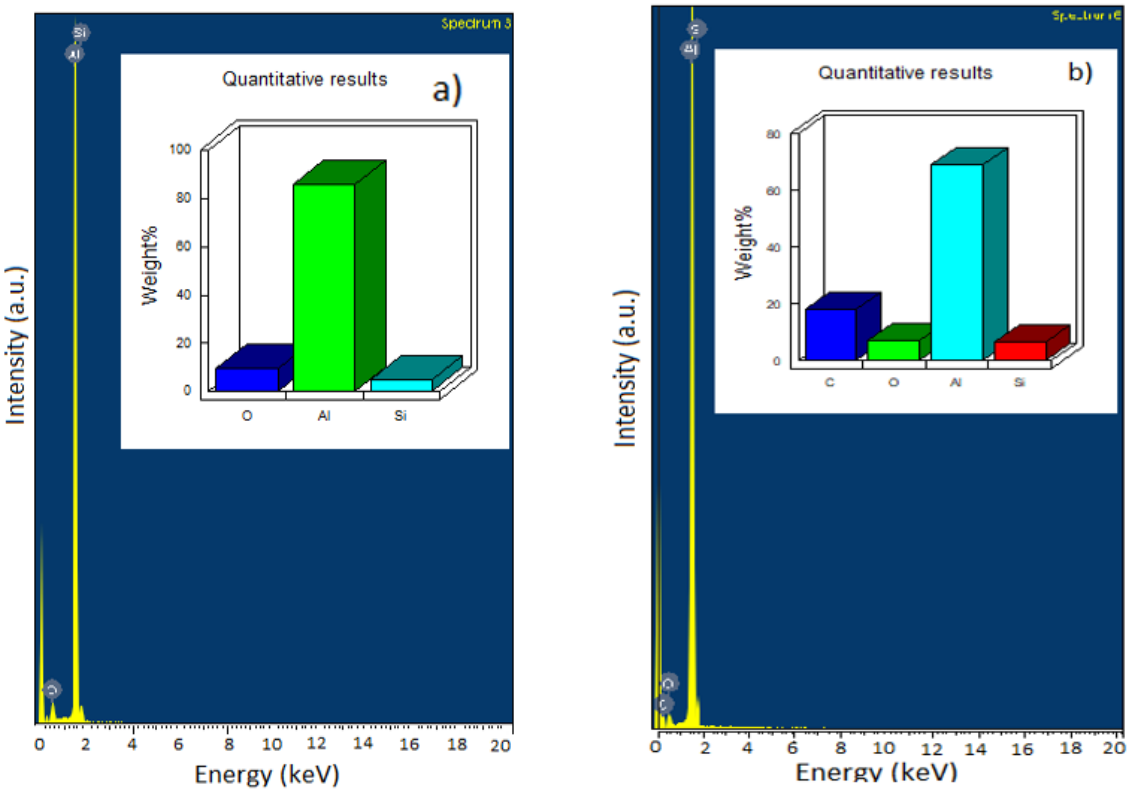

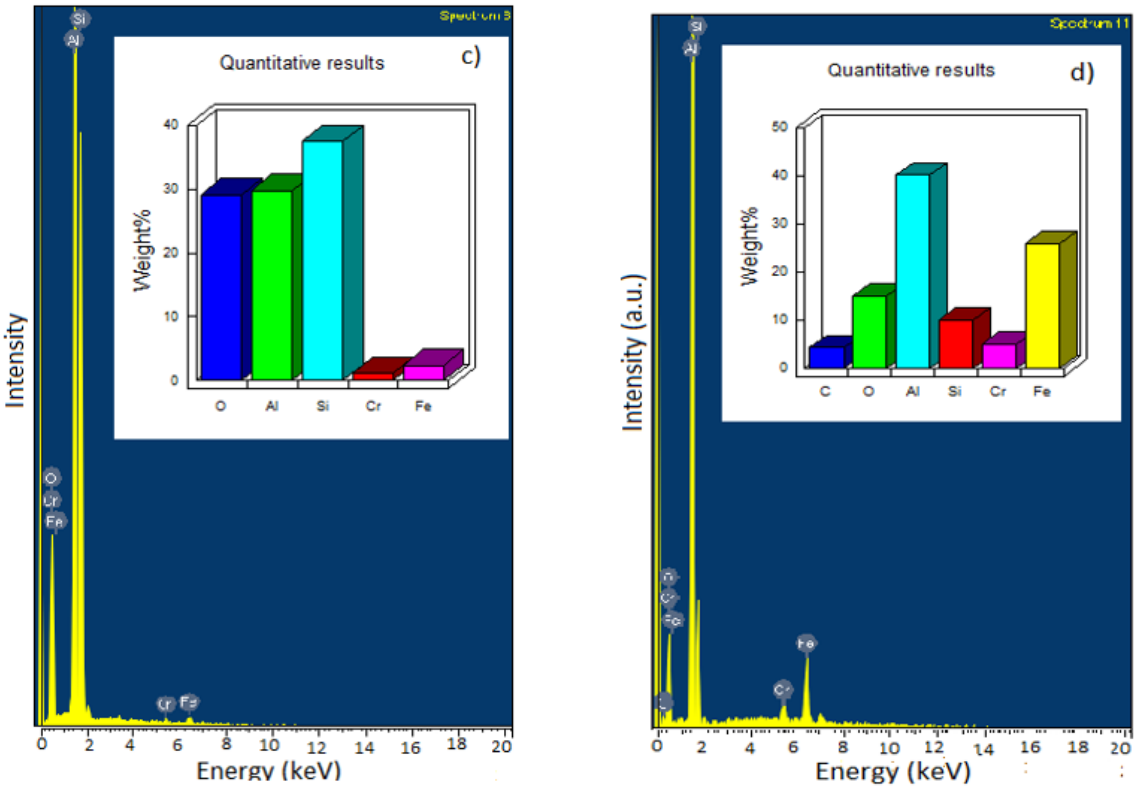

Figure 8. EDX analysis of corroded a) unreinforced A413 alloy, b) A413-5 wt.% SiC, c) A413-10 wt.% SiC, and d) A413-15 wt.% SiC composites.

Thus, for composite containing 5 % SiC, no pits can be observed, only a uniform type of corrosion at the metallic matrix surrounding the SiC particulates, Fig. 7 b. As the SiC contents increased to 10 or 15 %, the damaged surface area increased as shown in Figs. 7 c and d, where a selective attack at the metallic matrix next to the SiC reinforcement particulates can be observed. The justification of greater corrosion susceptibility of the composites containing either 10 or 15 % SiC in 3.5 wt% NaCl solution could be owing to discontinuity of the matrix material in the composites. The weak bonding between metallic matrix and SiC particulates will allow corrosion attack to start, and since these particulates will act as cathodes, surrounding metallic matrix will act as active anode. The sites where protective corrosion products film can be disrupted increase by increasing the SiC contents, and, thus, the number of places where corrosion can take place, with an increase in the corrosion rate [38].

EDX micro chemical analysis for unreinforced A413 alloy and composite containing 5 % SiC, Figs. 8 a and b, showed the presence of Al and O together with chemical elements contained in the SiC reinforcement particulates, Si or C. The high contents in both Al and O indicates the existence of the Al_2O_3 layer passive film which protects the alloy. However, for composites containing either 10 or 15 % SiC, Figs. 8 c and d, in addition to these chemical elements, some other elements present in the metallic A413 alloy, such as Cr and Fe, were detected. The contents of Al in this case was much lower than that detected for unreinforced A413 alloy or in the composite containing 5 % SiC, which might indicate a less protective layer of corrosion products. Also, the presence of Fe, which forms non

protective corrosion products, might have caused less protective corrosion products film on the composites, with an increase in their corrosion rates.

4. CONCLUSIONS

The effect of adding different SiC contents (5, 10, and 15 wt.%) in the A413 alloy by mechanically alloyed has been evaluated in 3.5 wt.% NaCl solution. It was found that both density and porosity of composites increased with the increase in the SiC contents. Electrochemical tests have shown that corrosion behavior was improved with the addition of 5% SiC but it was detrimental for higher SiC contents. Thus, polarization curves showed that the pitting potential value increased whereas both corrosion and passive current density values for composite containing 5% SiC as compared with unreinforced A413 alloy. The I_{corr} and I_{pas} values increased by increasing further the SiC contents whereas the pitting potential value decreased. Polarization resistance value of unreinforced A413 alloy increased for composite containing 5 or 10 % SiC but it decreased for composites containing 15 % SiC. It was found that corrosion product layer formed either in unreinforced A413 alloy or in the composite containing 5 % SiC consisted basically of protective Al2O3, whereas that formed on top of composites containing 10 or 15 % SiC were less protective, containing less amounts of Al together with Cr and Fe.

ACKNOWLEDGEMENTS
Ociel Rodriguez Pérez is thankful for the postdoctoral fellowship DGAPA-UNAM. Also, He would like to thank the Department of Metallurgical Engineering of the Faculty of Chemistry, UNAM for the facilities provided for the development of this project.

References

1. M. Baghi, B. Niroumand, and R. Emadi, *Journal of Alloys and Compounds*, 710 (2017) 29.
2. L. Bolzoni, M. Nowak, and N. Hari Babu, *Materials Science and Engineering A*, 628 (2015) 230.
3. R. Srinivasan, A. Ramesh, and A. Athithanambi, *Matereals Today*, 5 (2018) 13486.
4. R. Karuppasamy, Debabrata Barik, N.M. Sivaram, and Milon Selvam Dennison, *International Journal of Materials Engineering Innovation*, 11 (2020) 34.
5. V. Pawar, S. B. Chikalthankar, and V. Bhagat, *International Journal of Research in Engineering and Technololgy*, 5 (2018) 717.
6. M. S. Dastjerdi, A. Mokhtarian, and P. Saraeian, *Inernational Journal of Mechanical and Materials Engineering*, 15 (2020) 5.
7. R. Pandiyarajan, M.P. Prabakaran, T. Rajkumar, K. Vetrivel Kumar, and R. Manikandan, *Materials Today*, 37 (2021) 1794.
8. P. Mishra, P. Mishra, and R. S. Rana, *Materials Today*, 5 (2018) 6018.
9. T. Sridhara, H. R. Manohara, and T. Basava, *Materials Today*, 4 (2017) 10714.
10. O. Rodríguez Pérez, J. A. García-Hinojosa, F. J. Rodríguez Gómez, S. Mejia-Sintillo, V.M. Salinas-Bravo, R. Lopes-Sesenez, J.G. Gonzalez-Rodriguez and Cesar A. Garcia-Pérez, *International Journal of Electrochemical Science*, 14 (2019) 7423.
11. M. Arab, M. Azadi, and O. Mirzaee, *Materials Chemistry and Physics*, 253 (2020) 123259.
12. K.Ozturk, R. Gecu, and A. Karaaslam, *Ceramics International*, 47 (2021) 18274.

13. E.J. Moreno Carpintero, I. Santos Ramos, G. Rosas, M. A. Espinosa Medina, E. Sarmiento-Bustos, R. Lopez-Sesenes, and J.G. Gonzalez-Rodriguez, *Int. J. Electrochem. Sci*., 15 (2020) 3029.
14. A. E. Nassar, and E. E. Nassar, *Journal of King Saudi University Engineering and Science*, 29 (2017) 295.
15. E. Tekoğlu, D. Ağaoğulları, Y. Yürektürk, B. Bulut, and M. Lütfi Öveçoğlu, *Powder Technology*, 340 (2018) 473.
16. J. Rui-Song, W. Wen-Hu, S. Guo-Dong, and W. Zeng-Qiang, *Journal of Manufacturing Processes*, 23 (2016) 249.
17. Zhi-Guo Wang, Chuan-Peng Li, Hui-Yuan Wang, Jia-Ning Zhu, Cheng Wang, and Qi-Chuan Jiang, *Journal of Materials Engineering and Performance*, 26 (2016) 729.
18. Niveen Jamal Abdalkader, Payman Suhbat Ahmed, Mervit Mahdi Hanoos, and Satha Riyadh Ahmeb Izzat, *Zanco Journal of Pure and Applied Science*, 28 (2016) 251.
19. S. M. Mahdi, and L. Ghalib, *Journal of Bio and Tribo Corrosion*, 8 (2021) 8.
20. M. Aruna and S., Arivukkarasan, *International Journal of Applied Engineering Research,* 15(2020), 1-4.
21. A. Riquelme, P. Rodrigo, M. D. Escalera-Rodriguez and J. Rams, *Coatings, 11 (*2021) 639.
22. S. Sarapure, B. P. Shivakumar and M. B. Hanamantraygouda. *Journal of Bio- and Tribo-Corrosion*, 6 (2020) 31.
23. S.M. Almotairy, E.-S.M. Sherif, N.H. Alharthi, H.S. Abdo, H.F. Alharbi and M. Luqman. *Crystals*, 11 (2021) 1231.
24. R.T. Loto and P. Babalola, *Journal of Materials Research and Technology*, 8 (2 0 1 9) 2517.
25. P. Ajagol, B.N. Anjan, R.N. Marigoudar and P. Kumar, *IOP Conf. Series: Materials Science and Engineering* 376 (2018) 012057.
26. ASTM, G5-94. Annual book of ASTM standards. Standard reference test method for making potentiostatic and potentiodynamic anodic polarization measurements, 3(2000) 57–7.
27. M.F. Zawrah, W.M. El-Meligy, H.H.A. Saudi, S. Ramadan and M.A. Taha, *Biointerface Research in Applied Chemistry*, 12, (2022) 2068.
28. E.-S.M. Sherif, J. Potgieter, J. Comins, L. Cornish, P. Olubambi and C. Machio, *Corrosion Science*, 51 (2009) 1364.
29. W. Badawy, F. Al-Kharafi and A. El-Azab, *Corrosion Science,* 41(1999) 709.
30. A. Pardo, M.C. Merino, S. Merino, F. Viejo, M. Carboneras, R. Arrabal, *Corros. Sci.,* 47 (2005) 1750.
31. K. K. Alaneme, *Leonardo J. Sci*., 18 (2011) 55.
32. P.D. Reena Kumari, J. Nayak, A. Nityananda Shetty, *Arabian J Chem.,* 9 (2016) S1144.
33. A. Onat, *J Alloys Compd*., 489 (2010) 119.
34. Hosni Ezuber, A. El-Houd, F. EI-Shawesh, *Materials and Design,* 29 (2008) 801.
35. K. Jafarzadeh, T. Shahrabi, M.G. Hosseini, *J. Mater. Sci. Technol.,* 24 (2008) 215.
36. M.C. Pardo, R. Merino, F. Arrabal, M. Carboneras, *J. Electrochem. Soc*., 153 (2006) B52.
37. F. B. Growcock, R. J. Jasinski, *J. Electrochem. Soc.,* 136 (1989) 2310.
38. E.-S.M. Sherif and S.-M. Park, *Electrochimica Acta*, 51 (2006) 1313.